Tellus (1977), *29*, 561–571

A numerical study of the response of a barotropic ocean to a moving hurricane

By HAN-HSIUNG KUO[1] and TAKASHI ICHIYE, *Department of Oceanography, Texas A&M University, College Station, Tx. 77843, U.S.A.*

(Manuscript received April 12, 1976; in final form February 28, 1977)

ABSTRACT

The response of a barotropic ocean to a moving hurricane is studied numerically for a rectangular constant-depth ocean with a shelf on one side. The large-scale features of sea level and circulation changes are determined, though a meso-scale phenomenon like shelf waves is recognized on the shelf area. In the open sea the change of sea level is primarily due to the low pressure and the strong current results from the wind stress. The storm over the open sea is accompanied by forced waves and leaves behind a geostrophically balanced current. When the storm is far away from the shore, the coastal region experiences only a slight inertial-gravity oscillation. A sudden change of sea level and an increase in velocity occur as the storm passes over the shelf. After the storm goes ashore the forced waves become free shelf waves which travel along the coast clockwise. The numerical results are compared to the observed data on sea-level variation along the coast and on the temperature change in the ocean after the passage of a storm.

1. Introduction

After a hurricane is generated, it passes over the open sea, dashes through the continental slope and shelf, and proceeds inland. The responses of the ocean have been the subjects of many investigators. However, each one focused on a different aspect of the phenomena, such as the storm surge along the coast or the circulation in the deep water of the ocean.

Among studies on barotropic mode, Kajiura (1956) first treated an analytically steady-state response of a deep ocean of infinite extent to a hurricane moving with a constant speed [see Ichiye (1972) for detailed review]. For a closed ocean or near shore areas, either complicated boundaries or non-linear equations forced many workers to resort to numerical studies. Miyazaki (1965) treated storm surges in the Gulf of Mexico for a hurricane and Heaps (1969) in the North Sea for extra-tropical cyclones. Both used a realistic coastline and bottom topography, but linearized equations except the bottom friction terms by Miyazaki. Paskausky (1971) used a non-linear vorticity equation for determining circulation change in the Gulf of Mexico due to the passage of a hurricane but not for sea-level variations in the Gulf. Jelesnianski (1971) was mainly concerned with the distribution of surge heights along a shallow coast when a hurricane impinges on a continental shelf. Endoh (1973) discussed change of a western boundary current caused by a storm moving parallel to the coast in a rectangular ocean on the β-plane. Forristall (1974) studied the circulation near the coast due to a moving storm. However, there is no systematic study of a moving storm on the large ocean and the coastal region as a whole. The present study is an attempt to fill this gap.

Response of the ocean to a moving storm is a transient phenomenon. Our investigation will concentrate on the change of sea level and circulation due to a moving hurricane over a barotropic ocean. In the model, a hurricane moves with a constant speed from east to west in the middle of a rectangular, homogeneous basin. The basin has a continental shelf and slope on the western side.

Because the barotropic model is used in the present investigation, we have left out some

[1] Now at EG & G Idaho Inc., P.O. Box 1625, Idaho Falls, Idaho 83401, U.S.A.

important phenomena associated with a baroclinic ocean such as the intense upwelling under the center of a hurricane (Leipper, 1967; O'Brien & Reid, 1967) and the interaction between the barotropic and baroclinic modes near the continental slope (Rattray et al., 1969). These features occur at a smaller length scale than that of the barotropic response. A rather large grid interval was used in the present study in order to limit the computer time required for the numerical integration. Therefore the results do not represent those phenomena of smaller scales. It is not difficult to refine the present model to examine the responses of a baroclinic ocean.

First, a hurricane model and the governing equations are presented. The procedures used in numerical integration will be discussed next. According to the numerical results, the low pressure mainly causes the rise of sea level whereas the wind stress generates an intense current. As the hurricane moves over the open sea, a forced wave accompanies it and a geostrophically balanced current is left behind. When the storm is far from the shore, the sea level of the coastal region oscillates because of inertial gravity waves which are amplified by the continental slope and shelf. As the storm approaches the coast, the sea level changes suddenly and the current speeds also increase. After the hurricane moves inland, the forced waves will propagate as waves along the coast. Due to the effects of Coriolis force, the southward waves moving to the left of the storm have more energy than ones moving to the right. Consequently, the peak of sea-level anomaly moves southward along the western shelf as shelf waves (Adams & Buchwald, 1968).

2. The model

We assume that a hurricane is moving from east to west in the middle of a basin (2000 km by 2000 km). The basin has a continental shelf and slope at the west side. The depth of the basin (H) varies only in the x-direction (west to east). The profile is expressed as

$$H = H_a \cdot \{(1 - a) + a \cdot \tanh[(x - x_a)/x_w]\} \qquad (1)$$

where $H_a = 4000$ m, $a = 0.50061$, $x_a = 150$ km and $x_w = 50$ km. This gives a depth of 5 m at the shore and 4000 m for the ocean. The width of the continental shelf and slope is 200 km (Fig. 1).

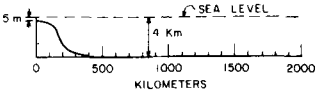

Fig. 1. The basin depth profile.

The response of the ocean is assumed to be barotropic. The two-dimensional Navier-Stokes equations governing the vertically averaged velocities in cartesian coordinates are

$$\frac{\partial \vec{u}}{\partial t} + \vec{u} \cdot \nabla \vec{u} + f\vec{k}x\vec{u} = -\frac{g}{\rho}\nabla\xi + A\nabla^2\vec{u} - \frac{K}{H} \cdot \vec{u} - \frac{1}{\rho}\nabla p + \frac{1}{\rho H}\vec{\tau} \qquad (2)$$

$$\frac{\partial \xi}{\partial t} + \nabla \cdot (H\vec{u}) = 0 \qquad (3)$$

where u, v are velocities in the x,y-directions respectively (positive in eastward and northward); g, gravitational acceleration; ξ, sea level; f, Coriolis parameter; A, horizontal kinematic eddy viscosity; K, bottom frictional coefficient; ρ, density of the sea water; p, the pressure of the hurricane; and $\vec{\tau}$, the wind stress associated with it. Both the bottom friction and horizontal eddy viscosity are introduced in the model. The bottom friction is assumed proportional linearly to the velocity. Further, the amplitude effect is neglected by taking the total depth as H instead of $H + \xi$.

The hurricane structure used in the present study is taken from the model by Schloemer (1954). It is located at the center of the eastern boundary of the basin and moves westward. The pressure (p) of the hurricane is

$$p = p_0 - (p_n - p_0) \cdot \exp\{-R_m/[(x - x_0 - V_x t)^2 + (y - y_0 - V_y t)^2]^{\frac{1}{2}}\} \qquad (4)$$

where p_0 is the center pressure; p_n, the asymptotic pressure at the outer periphery of the hurricane; R_m, the distance at which the maximum gradient wind speed occurs; (x_0, y_0), the initial position of the hurricane; (V_x, V_y), the speed of the moving hurricane. The wind stress ($\vec{\tau}$) of the hurricane is calculated by the relation (Roll, 1965).

$$\vec{\tau} = \rho_a C_D |V_w| V_w \qquad (5)$$

where ρ_a is the air density; C_D, the drag coefficient; and $\vec{V}_w$, the velocity of the wind. The friction-free wind speed (V) is calculated from the cyclo-

strophic wind equation $V^2 = (r/\rho_a)\partial p/\partial r$ where r is a radius from a moving center of the storm. The wind speed in (5) is taken as 70% of the friction-free wind speed V. The direction of the wind is deflected by 35° inward from the isobar.

The boundary conditions impose a vertical wall on four sides where there is no normal flux. Besides no slip conditions are applied except on the east coast, where the sea level is assumed to be in equilibrium with the atmospheric pressure. Thus

$$\text{(i)}\ \vec{u} = 0 \quad \text{at } y = 0, y = 2000 \text{ km}, \text{ at } x = 0$$

$$\text{(ii)}\ u = 0, \quad \xi \to \xi_0 \text{ (static sea level) as } x \to 2000 \text{ km} \tag{6}$$

Because of condition (ii), only the shelf waves on the western side are taken into consideration. This condition also suppresses Kelvin waves which may be generated on the east coast, as indicated in numerical works of Suginohara (1973) since these waves are not the main subject of the present study.

Equations (2), together with boundary conditions (6), are solved as an initial value problem by numerical integration. The values of the parameters used in the calculation are given in Table 1.

3. Numerical procedures

Since the depth variation is greatest near the western coast, a closely spaced grid system is desirable to give a high resolution for the dynamical variables in this region. A non-uniform grid in the x-direction is used in the numerical calculation. The positions of the grid points are determined by the stretching coordinate (η) as

$$x = L(\eta^2)$$

where L is the length of the basin in the x-direction (2000 km) and η varies uniformly from 0 to 1.0. The properties of these non-uniform grids have been studied by de Rivas (1972).

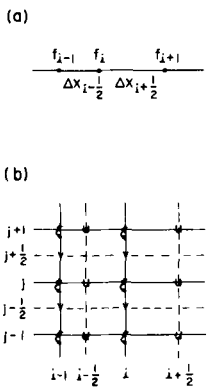

Fig. 2. (a) The locations of the variables for the definitions of average and derivative. (b) Arrangement of the dynamical variables.

The following notation will be used (cf. Fig. 2a):

$$\bar{f}_i^x = (\Delta x_{i+\frac{1}{2}} + \Delta x_{i-\frac{1}{2}})^{-1}[\Delta x_{i+\frac{1}{2}} f_{i-1} + \Delta x_{i-\frac{1}{2}} f_{i+1}]$$

$$\bar{f}_i^{xx} = (\Delta x_{i+\frac{1}{2}} + \Delta x_{i-\frac{1}{2}})^{-1}[(\Delta x_{i+\frac{1}{2}} + \Delta x_{i-\frac{1}{2}}) f_i + \Delta x_{i+\frac{1}{2}} f_{i-1} + \Delta x_{i-\frac{1}{2}} f_{i+1}]/2$$

$$f_x = \partial f_i/\partial x = [(\Delta x_{i+\frac{1}{2}} \cdot \Delta x_{i-\frac{1}{2}}) \cdot (\Delta x_{i+\frac{1}{2}} + \Delta x_{i-\frac{1}{2}})]^{-1} \times [(\Delta x_{i-\frac{1}{2}})^2 (f_{i+1} - f_i) + (\Delta x_{i+\frac{1}{2}})^2 \cdot (f_i - f_{i-1})]$$

and

$$f_{xx} = \frac{\partial^2 f_i}{\partial x^2} = [\tfrac{1}{2}\Delta x_{i+\frac{1}{2}} \cdot \Delta x_{i-\frac{1}{2}} (\Delta x_{i+\frac{1}{2}} + \Delta x_{i-\frac{1}{2}})]^{-1} \times [\Delta x_{i-\frac{1}{2}} \cdot (f_{i+1} - f_i) - \Delta x_{i+\frac{1}{2}} \cdot (f_i - f_{i-1})] \tag{7}$$

Table 1. *Values of parameters*

Parameters	Value	Parameters	Value
f	$6.15 \times 10^{-5}\ s^{-1}$	g	$9.80\ m \cdot s^{-2}$
A	$6 \times 10^6\ cm^2\ s^{-1}$	K	$1 \times 10^{-2}\ s^{-1}$
ρ	$1\ kg \cdot m^{-3}$	ρ_a	$1.226 \times 10^{-3}\ kg \cdot m^{-3}$
p_0	930 mb	p_n	1030 mb
x_0	2000 km	y_0	1000 km
V_x	$-5\ ms^{-1}$	V_y	0·0
R_m	50 km	C_D	2.37×10^{-3}

The finite difference form of eqs. (2), using a generalized Arakawa scheme (Grammeltvedt, 1970) and with the DuFort-Frankel finite-difference approximation for the viscous terms (Richthyer & Morton, 1967), can be written as

$$\bar{u}_t^t + \tfrac{1}{3}\{(\bar{u}^x\bar{u}^x)_x + \tfrac{1}{2}[u(u + 4\bar{u}^{xx} + 4\bar{u}^{yy} - 8u)]_x^x$$
$$+ [2\bar{v}^{xy}\bar{u}_y^y + \bar{v}^x u_y^y]\} - f\bar{v}^{xy} = -\frac{g}{\rho}\xi_x$$
$$+ A(\bar{u}_{xx}^{2t} + \bar{u}_{yy}^{2t}) - K\bar{u}^{2t}/\bar{h}^x - P_x + \tau_x/\bar{h}^x$$
$$\bar{v}_t^t + \tfrac{1}{3}\{2\bar{u}^{xy}\bar{v}_x^x + \bar{v}^y v_x^x + (\bar{v}^y\bar{v}^y)_y$$
$$+ \tfrac{1}{2}[v(v + 4\bar{v}^{xx} + 4\bar{v}^{yy} - 8v)]_y^y\} + f\bar{u}^{xy} = -\frac{g}{\rho}\xi_y$$
$$+ A(u_{xx}^{2t} + \bar{v}_{yy}^{2t}) - K\bar{v}^{2t}/\bar{h}^y - P_y + \tau_y/\bar{h}^y$$
$$\xi_t^t + [(\bar{h}^x u]_x + (\bar{h}^y v_y)] = 0 \qquad (8)$$

(cf. Fig. 2b). This finite-difference scheme conserves the kinetic energy, total water volume, mean vorticity, and mean square vorticity for non-divergent flow. The linear stability condition for the present scheme reads $C(\Delta T/\Delta L) \leq 1/2$ for $V_c \ll C$, where $C = (gH)^{1/2}$; ΔT, the time increment for each step; ΔL, the grid interval; V_c, the characteristic velocity of the flow. A grid system of 23 × 23 (mesh point 45 × 45) was used in the present calculation. The smallest grid interval in the x-direction is 5 km, the largest is 195 km. The interval in the y-direction is 100 km uniformly. With a time step of 90 s, this proves satisfactory. The boundary condition (ii) of (6) is incorporated by setting $\xi = 0$ at x far outside the basin. The integration starts at $t = 0$ when the hurricane is suddenly introduced at the center of the eastern boundary. It stops at $t =$ 144 hours, when the storm disappears inland.

In the present model, the wind stress is treated as a body force and thus it appears as divided by the depth in eqs. (2). Consequently, this force becomes quite large when the hurricane moves near the coastal area where the water is shallow. This large body force makes the numerical calculation unstable near the coast unless much finer grids are used there. Therefore the value $(\vec{\tau}/H)$ of each wind stress component is limited to $2\rho f u^*$, where u^* is the characteristic velocity based on the balance of Coriolis force and the pressure field of the hurricane. With the choice of parameters given in Table 1, the value of u^* is 7.91 cm s^{-1}. This limits the wind speed at the west coast below 4.3 m/s and at 10 km off the coast (third grid points from the coast) below 10 m/s. Although limitation of wind speed at the coast seems to be highly artificial, in an actual situation the water motion adjacent to the coast is influenced strongly by bottom friction and turbulence. Therefore this artificial limitation should be interpreted as manifest of strong dissipation mechanism near the coast of the real ocean. With this grid system, the model could not duplicate small-scale features of surges near the coast as studied by Harris (1963). Therefore it is not useful to introduce a more realistic non-linear bottom friction law or finite amplitude effect on the equation of continuity. Our present concern is mainly with features of scales of a hurricane and not of small scales.

4. Results and discussion

The hurricane model used in the calculation yields a pressure drop of 100 mb between the center and outer region, a maximum wind speed of 62.5 ms^{-1} and wind stress of 11.5 Newton m^{-2} (10^{-2} mb). A sea-level change due to the pressure drop will be 101 cm according to the inverted barometric effect. The response of the open sea to the pressure and wind stress will be examined first. The effect of a moving hurricane is a combination of the pressure and wind stress. Figs. 3 and 4 show the

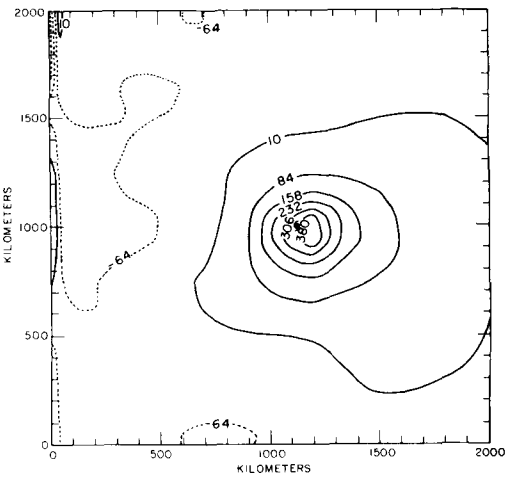

Fig. 3. Sea level (in mm) due to the pressure of the moving hurricane at 48 hours. Full lines are for elevation, dotted lines for depression. The highest is 455 mm and the lowest is −286 mm. The contour interval is 74 mm.

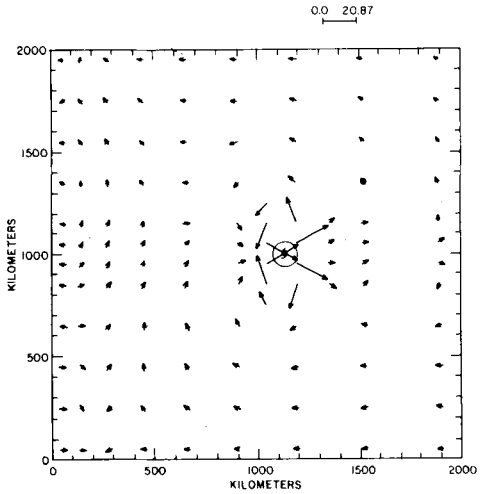

Fig. 4. Transport vector (in 10 m^3 s^{-1} per m) of the ocean circulation due to the pressure of a moving hurricane at 48 hours. A circle around the hurricane center indicates the maximum gradient wind radius.

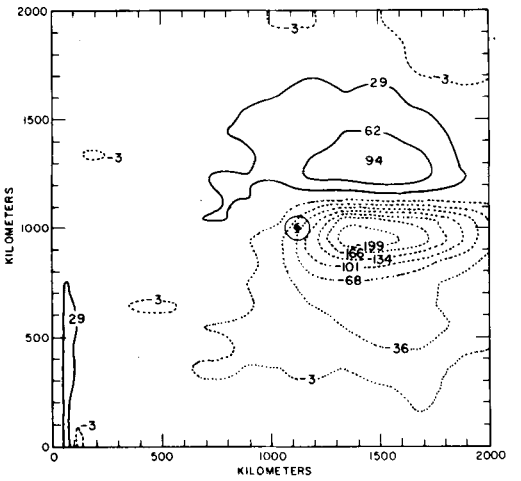

Fig. 5. Sea level (in mm) due to the wind stress of a moving hurricane at 48 hours. The full lines are for elevation and dotted lines are for depression. The highest is 94 mm and the lowest is −251 mm. The contour interval is 33 mm. A circle around the hurricane center indicates the maximum gradient wind radius.

sea level and current transport ($H\vec{u}$) due to pressure at 48 hours after the integration begun. The hurricane is located (1136 km, 1000 km), near the center of the basin. The sea level of forced waves induced by the low pressure distribution has a maximum height of 45 cm under the center of the hurricane. It is less than half the value of the steady response due to the inverted barometric effect. There is also a depression of the free surface ahead of the hurricane. The water in front of the advancing hurricane flows into the center of the storm in anticipation of the rise of water level. The water behind the hurricane flows out of the center as the sea-level subsides. The moving pressure system generates a two-gyre circulation pattern. The effect of wind stress is quite different. Figs. 5 and 6 give the sea level and circulation due to wind stress at the same time. A geostrophically balanced situation exists after the passage of the storm. The result is similar to that of the steady response of a moving hurricane obtained by Kajiura (1956). However, the present calculations also show that the water level to the north of the storm rises slightly (see appendix for detailed discussion of the comparison with Kajiura's results). Circulation due to the wind stress is an elongated gyre. The response of a moving hurricane is quite different from that of a stationary hurricane as studied by O'Brien & Reid (1967). They assumed that all

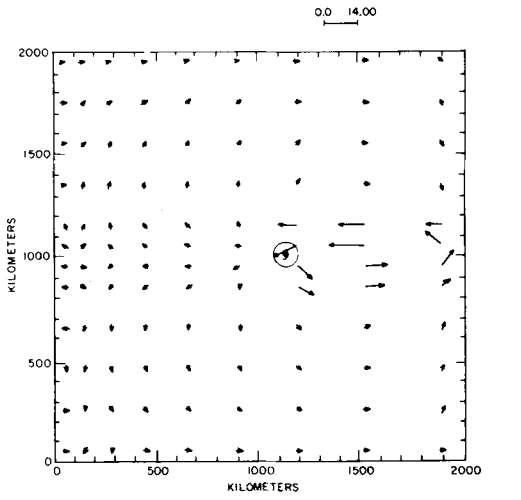

Fig. 6. Transport vector (in 10 m^3 s^{-1} per m) of the ocean circulation due to the wind stress of a moving hurricane at 48 hours.

the dynamical variables were axially symmetric. As a consequence, circulation is always a cyclonic gyre under the center of the storm.

Figs. 7 and 8 denote the mass transport and sea level due to both wind and pressure effects at 110 hours, when the hurricane is located (20 km, 1000 km) off the shore. The wind-induced current

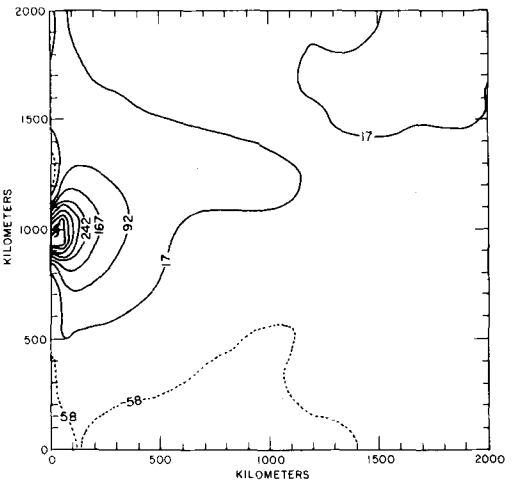

Fig. 7. Sea level (in mm) due to the pressure and the wind stress of a moving hurricane at 110 hours. The full lines are for elevation and the dotted lines are for depression. The highest is 617 mm and the lowest is −73 mm. The contour interval is 75 mm.

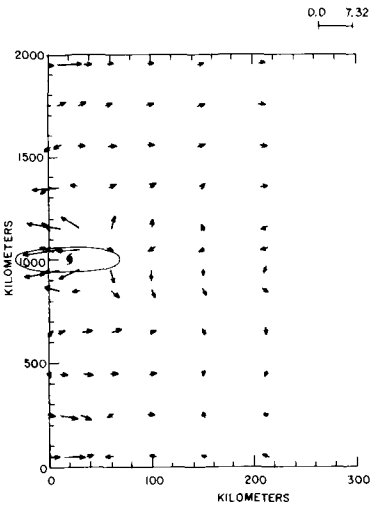

Fig. 9. Velocity vector (in 10^{-2} m s^{-1}) near the coast due to the pressure of a moving hurricane at 110 hours. An ellipse around the hurricane center indicates the maximum gradient wind zone.

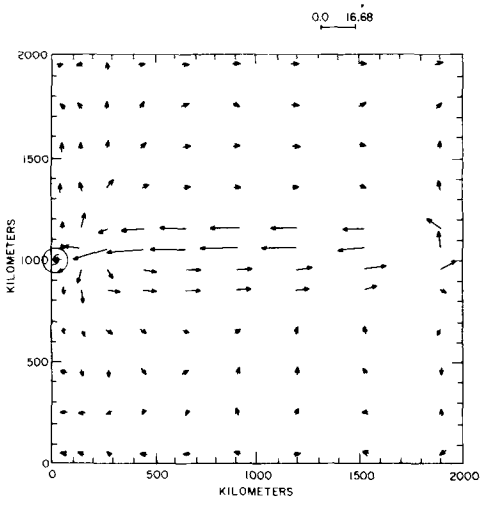

Fig. 8. The transport vector (in 10 m^3 sec^{-1} per m) of the ocean circulation due to the pressure and the wind stress of a moving hurricane at 110 hours. A circle around the hurricane center indicates the maximum gradient wind radius.

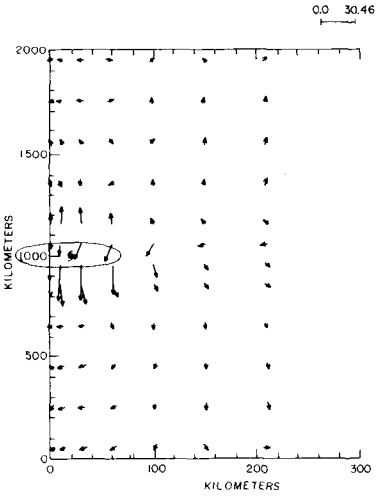

Fig. 10. Velocity vector near the coast due to the wind stress of a moving hurricane at 110 hours. An ellipse around the hurricane center indicates the maximum gradient wind zone.

extends near the path of the hurricane over the basin. The sea level rises to a maximum of 61.7 cm near the shore. It is interesting to investigate separately the velocities associated with the pressure (Fig. 9) and with the wind stress (Fig. 10) near the shore. The water movement due to the pressure effect is with the hurricane and the wind-induced current flows more or less along the coastline. The maximum velocity of the wind-generated current (30.46 cm s^{-1}) is four times as large as the pressure-induced maximum velocity (7.32 cm s^{-1}). As the hurricane moves inland, the forced waves will then behave as free edge waves propagating

along the shelf. Because of the Coriolis force, the southward-moving waves have a larger fraction of the total energy than the northward waves (Reid, 1958; Kajiura, 1958). Southward velocity transport is larger than the northward transport, as indicated by Figs. 8 and 10. The maximun height of sea level will propagate southward. Fig. 11 shows the sea level after 124 hours of integration time when the hurricane is inland (−232 km, 1000 km). The maximum rise of sea level (50.1 cm) occurs about 150 km south of the path of the hurricane.

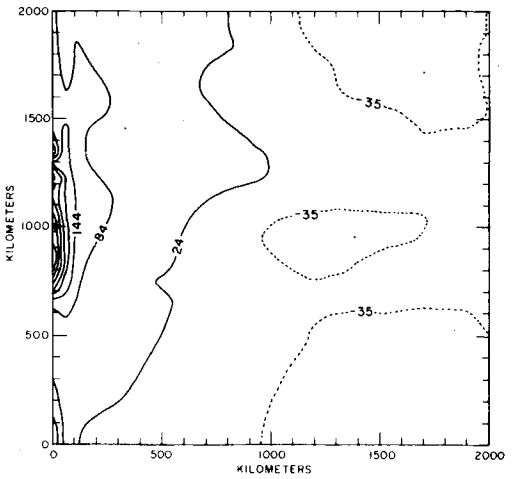

Fig. 11. Sea level (in mm) due to the pressure and wind stress of a moving hurricane at 124 hours. The full lines are for elevation and the dotted lines are for depression. The highest is 501 mm and the lowest is −95 mm. The contour interval is 60 mm.

The surge along the coast can best be viewed by sea-level changes with time at points A (5 km, 1050 km), B (5 km, 850 km) and C (5 km, 1250 km) shown in Fig. 12. At point A, the hurricane path is 50 km south; the maximum surge occurs at the time when the storm passes the point. The effect of the Coriolis force is evident in the surge heights at points B and C. They have a rather broad peak and the highest surge occurs about 12 hours after the passage of the storm. One should also notice that the hurricane will not influence the shore region until it moves near the continental slope and shelf. Fig. 13 gives time series plots of velocities at two points. One (D) is in the deep basin (695 km, 950 km); and the other (E) at the continental shelf (61.5 km, 950 km). In the deep basin the current is not significant until the hurricane passes. After passage of the storm a geostrophically balanced current is generated. Before the hurricane approaches, small amplitude inertial gravity waves appear over the shelf region. This oscillation is best manifested in the x-component of the velocity (u) which is amplified by the continental shelf. It can also be noticed in Fig. 12. The velocity builds up rapidly when the storm approaches, as indicated at E in Fig. 13.

5. Concluding remarks

The numerical results of this study of a moving storm on a barotropic ocean give a bird's-eye view of the change of sea level and circulation over the

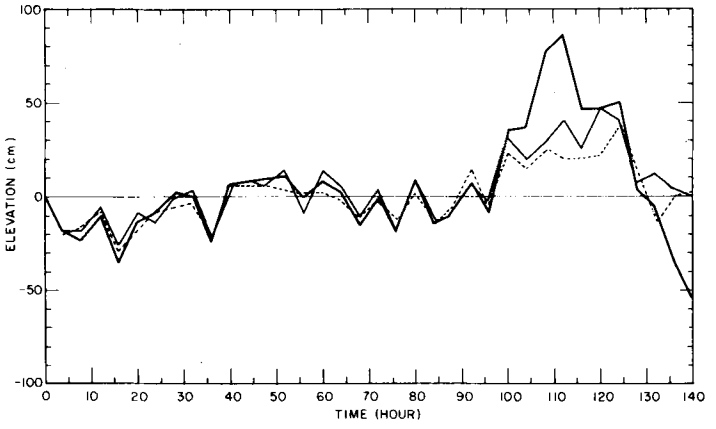

Fig. 12. Time series plots of the sea levels due to pressure and wind stress of a moving hurricane at points A (5 km, 1050 km) in heavy line, B (5 km, 850 km) in thin line, and C (5 km, 1250 km) in dotted line.

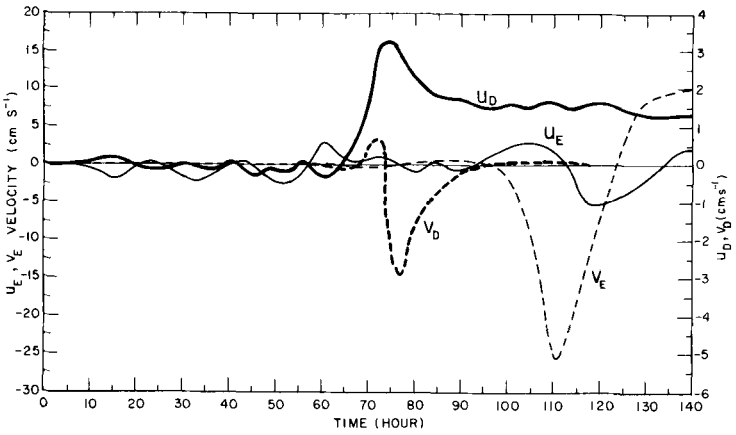

Fig. 13. Time series plots of velocity at point D (695 km, 950 km) in deep basin and at point E (61.5 km, 950 km) over continental shelf.

open sea and coastal region. The surge along the coast is primarily due to the low pressure and the strong current is the result of the wind stress. The elongated gyre of the geostrophically balanced current after the passage of a storm in the mid-ocean may qualitatively explain observed sea surface temperature changes before and after a hurricane, though quantitative discussion should take into account the baroclinic mode. Leipper (1967) and Jordan (1964) observed that the change of sea surface temperature is represented by an elliptic cold area along the path of the hurricane. Leipper (1967) also reported that the center of the cold water area moves to the left (westward) near the coast in the Gulf of Mexico after the hurricane passes through. The present model clearly indicates a strong southward transport near the west coast, although it is necessary to interpret our results in terms of the upper layer transport in order to correlate to a cold water region.

The southward movement of high sea level along the western coast in this model can be favorably compared with the results of Isozaki (1968) and Ichiye et al. (1973). The former studied sea-level anomalies along the west coast of Japanese islands during the passage of typhoons over the Japan Sea. He found that the anomaly peak moved northeastward with speeds of 3–4 m s^{-1} as shelf waves (Adams & Buchwald, 1969; Gill & Schumann, 1974). (The coast is on the southeast side of the Japan Sea.) The latter studied the sea-level anomalies along the Gulf coast due to Hurricane Celia which landed between Galveston and Port Isabel, Texas, in August 1970. They found that the maximum anomaly moved southward with a speed of about 5 m s^{-1}. The present result shows that the peak moves southward along the western coast with a speed of about 4.5 m s^{-1}. Since out model used reduced wind stress near the coast, the magnitude of the shelf wave peak may not compare with observed data but agreement in moving speed is convincing.

6. Acknowledgement

The authors are grateful to the National Center for Atmospheric Research (operated with support from the National Science Foundation) for providing us with the computer time required in this study. The research is supported by the National Science Foundation under Grant OCE 76-14995 and by Office of Naval Research Contract N00014-75-C-0537.

7. Appendix

The mid-ocean responses illustrated with Figs. 3 to 6 can be compared with the analytical model studied by Kajiura (1956). The maximum velocity obtained by the present calculation is about 5 cm/s from Fig. 4. Thus, when the characteristic distance is taken as 50 km, the radius of maximum wind speed, the ratio of inertial force to Coriolis force (Rossby number) is 0.01. Therefore the non-linear

terms in the momentum eq. (2) can be neglected with an error of 2% even if the maximum speed is doubled. Similarly the ratios of eddy viscosity and bottom friction term to the Coriolis term are 4×10^{-3} and 4×10^{-4}, respectively. Therefore, frictional effects can be discarded.

The evaluation due to the linearized equations of motion and continuity can be given by the sum of ξ_1 and ξ_2 with

$$\frac{\partial^2 \xi_1}{\partial t^2} + f^2 \xi_1 = gH\nabla^2(\xi_1 - \bar{\xi}) - \text{div}\, \vec{\tau}/\rho \qquad \text{(A1)}$$

$$\frac{\partial^2 \xi_2}{\partial t^2} + f^2 \xi_2 = gH\nabla^2 \xi_2 - \int_0^t f\, \text{curl}\, \frac{\vec{\tau}}{\rho} dt \qquad \text{(A2)}$$

where $\bar{\xi}$ is the inverted barometric elevation.

Scaling of eq. (A1) by use of a horizontal distance scale R_m and a time scale $R_m/|V_x|$ indicates that the left-hand side terms of (A1) and (A2) are smaller by two orders of magnitude than the term with gH on the right-hand side. Therefore to the same order of errors produced by omission of non-linear and frictional terms, ξ_1 and ξ_2 can be expressed by solutions of the equations resulting from vanishing of the left-hand side of (A1) and (A2). Therefore the elevation due to the low pressure only can be given by $\bar{\xi}$. (This can also be interpreted that the initial elevation $\bar{\xi}$ is dissipated by propagating in two-dimensions with the speed of long waves, $\sqrt{gH}$). The maximum elevation shown in Fig. 3 is less than half that of $\bar{\xi}$. This may be due partly to a coarse grid in the present numerical scheme and partly to time-dependence. In fact, the distribution of $\bar{\xi}/\xi_{\max} = (1 - e^{R_m/r})$ is plotted in Fig. (A1) against the scale distance $r_* = r/R_m$ and this indicates that $\bar{\xi}$ becomes only about 63% of the maximum at 50 km from the center of the hurricane.

However, there is still a difference between the results of the present calculation and Kajiura's linear model due to several factors neglected in the latter. For the sea-level rise due to the pressure effect, the elevation is determined as a function of a radius from the storm center from Fig. 3 by assuming circles of the same area as that enclosed by the isobaths in Fig. 3. The central elevation is obtained as 74 cm by curve fitting. The normalized elevations with this value are plotted against r_* in Fig. A1. Although the trend of the curves agree, the central value is again about 70% of the theoretical

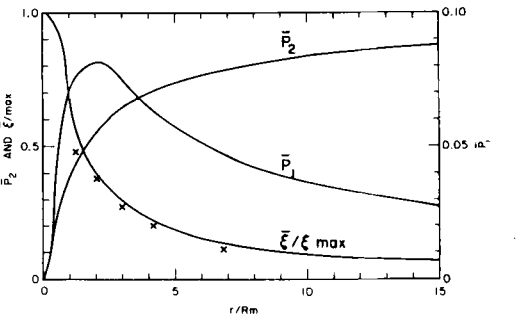

Fig. A1. Plots of $\bar{\xi}/\xi_{\max}$, $\bar{p}_1$, and $\bar{p}_2$ as functions of (r/R_m). Crosses represent values determined from numerical results in the text.

value. Such disagreement is more conspicuous in the transport field.

Kajiura derived the transport due to the low pressure effect as

$$Q_{1x}/V_x = -(\xi_1/2 + p_1 \cos 2\theta - p_2 \sin\theta) \qquad \text{(A3)}$$

$$Q_{1y}/V_x = -p_1 \sin 2\theta + p_2 \sin\theta \qquad \text{(A4)}$$

where θ is an angle from the positive x-axis and p_1 and p_2 can be given by

$$p_1 = -\xi_1 2^{-1} + r^{-2} \int_0^r r_0 \xi_1 dr_0 \qquad \text{(A5)}$$

$$p_2 = f(V_x r)^{-1} \int_\infty^r r_0 \xi_1 dr_0 \qquad \text{(A6)}$$

Taking $\xi_1 = \bar{\xi}$, one obtains

$$P_1/\xi_{\max} = 2^{-1} r_1 \{e^{-r_1} - r_1 E_1(r_1)\} = \bar{p}_1 \qquad \text{(A7)}$$

$$p_2/\xi_{\max} = fR_m V_x^{-1} \bar{p}_2;$$
$$\bar{p}_2 = 2^{-1}\{r_* - e^{-r_1}(r_*^{-1}) - r_1 E_1(r_1)\} \qquad \text{(A8)}$$

where

$$E_1(x) = \int_x^\infty t^{-1} e^{-t} dt \qquad \text{(A9)}$$

and

$$r_* = r/R_m; \quad r_1 = r_*^{-1} \qquad \text{(A10a,b)}$$

The function $\bar{p}_1$ and $\bar{p}_2$ are plotted against r_* in Fig. A1. In eqs. (A3) and (A4), the p_1 and p_2 terms represent the double and single cell circulation, respectively. The latter is in geostrophic balance with the pressure-induced elevation. Since the factor $fR_m/V_x = 0.615$ from Table 1, p_1 is less than

$\frac{1}{4}$ of p_2. Therefore the linear theory predicts pressure-induced single cell circulation, whereas the numerical result of Fig. 3 shows double cells. This is due to amplification of the p_1 terms by the nonlinear effects.

The wind-induced elevation also shows the difference between the present model (Fig. 4) and Kajiura's result, since the latter shows uniform depression behind the storm. However, this difference can be explained by the linear model, including the wind stress convergence which was omitted by Kajiura. The present wind stress magnitude is given by

$$T = \tau/\rho = \tau_m r_1 \exp(1 - r_1) \tag{A11}$$

where τ_m is the maximum value of τ/ρ at $r_* = 1$.

Solution of A1 (with the left-hand side being zero) for the wind stress of magnitude given by (A11) with angle ϕ inward can be expressed by

$$\xi_{1,w} = \tau_m (gH)^{-1} \sin\phi R_m e^{-1}\{E_1(r_*^{-1}) - E_1(r_m^{-1})\} \tag{A12}$$

where r_m is the scaled distance from the storm center to the nearest coast. The sea surface elevation due to the wind stress curl is also given approximately by a solution of (A2) as

$$\xi_2 = V_x^{-1} \int_x^{x_0} w\, dx \tag{A13}$$

where x_0 is the coordinate of the eastern (right-hand side) coast and w is given by

$$w = -f\tau_m (gH)^{-1} R_m e^{-1}\{E_1(r_*^{-1}) - E_1(r_m^{-1})\} \tag{A14}$$

It is seen immediately that the function $\xi_{1,w}$ is positive, whereas ξ_2 is negative. The amplitude of $\xi_{1,w}$ and ξ_2 are $\tau_m \sin\phi R_m/gH$ and $f\tau_m \cos\phi\,(x_0 - x)R_m/gHV_x$, respectively, and thus their ratio is $\tan\phi \cdot V_x/f(x_0 - x) = 0.54$ for $\phi = 35°$ and $x_0 - x = 864$ km. The veering of $\xi_{1,w}$ to the north (positive y-direction) is caused by the geostrophic current due to the positive and almost concentric nature of the isobaths of $\xi_{1,w}$ in contrast to the negative and trailing contours of ξ_2.

REFERENCES

Adams, J. K. & Buchwald, V. T. (1969). The generation of continental shelf waves. *J. of Fluid Mech. 35,* 815–826.

Endoh, M. 1973. A numerical experiment on the variations of western boundary current. Part II. Response to a moving typhoon. *J. Oceanog. Soc. Japan 29,* 28–43.

Forristall, G. Z. 1974. Three-dimensional structure of storm generated current. *J. of Geophys. Res. 79,* (18), 2721–2729.

Geisler, J. E. 1970. Linear theory of the response of a two-layer ocean to a moving hurricane. *Geophys. Fluid Dyn. 1,* 249–272.

Gill, A. E. & Schumann, E. H. 1974. The generation of long shelf waves by the wind. *J. of Phys. Oceanog. 4,* 83–90.

Grammeltvedt, A. 1970. A survey of finite difference schemes for the primitive equation for the barotropic fluid. *Mon. Weather Rev. 97* (3), 384–404.

Harris, D. L. 1963. *Characteristics of the hurricane storm surge.* U.S. Weather Bureau Technical Paper No. 48, 139 pp.

Heaps, N. S. 1969. A two-dimensional numerical sea model. *Phil. Trans. Roy. Soc. London A 265,* 93–137.

Ichiye, T. 1972. Circulation changes caused by hurricanes. *Contributions on the physical oceanography of the Gulf of Mexico* (ed. L. Capurro and J. L. Reid). Gulf Publishing Co., pp. 229–257.

Ichiye, T., Kuo, H. H. & Carnes, M. 1973. *Assessment of currents and hydrography of the Eastern Gulf of Mexico.* Dept. of Oceanography, Texas A&M University, Contribution No. 601, 326 pp.

Isozaki, I. 1969. An investigation on the variations of sea level due to meteorological disturbances on the coast of Japanese Island (IV). *J. Oceanog. Soc. Japan 25* (4), 191–200.

Jelesnianski, C. P. 1971. Bottom stress time-history in linearized equations of motion for storm surges. *Mon. Weather Rev. 98* (6), 461–478.

Jordan, C. L. 1964. *On the influence of tropical cyclones on the sea surface temperature field.* Proc. Symp. Trop. Meteor., New Zeland Meteor. Service, Wellington, pp. 614–622.

Kajiura, K. 1956. *A forced wave caused by atmospheric disturbances in deep water.* Technical Report 133-1, Department of Oceanography and Meteorology, Texas A&M University, 32 pp.

Kajiura, K. 1958. Effects of Coriolis force on edge waves. II. Specific examples of free and forced waves. *J. Marine Res. 16,* 144–157.

Leipper, D. F. 1967. Observed ocean condition and hurricane Hilda, 1964. *J. of Atmos. Sci. 24,* 182–196.

Miyazaki, M. 1965. A numerical computation of the storm surge of Hurricane Carla, 1961, in the Gulf of Mexico. *Oceanogr. Mag. 17* (1–2), 109–140.

O'Brien, J. J. & Reid, R. 1967. The non-linear response of a two-layer, baroclinic ocean to a stationary axially-symmetric hurricane: Part I. Upwelling induced by momentum transfer. *J. of Atmos. Sci. 24,* 197–207.

Rattray, M., Jr., Dworski, J. G. & Kovala, P. E. 1969. Generation of long internal waves at continental slope. *Deep-Sea Research,* Supplement 16, 179–195.

Reid, R. O. 1958. Effect of Coriolis force on edge waves (I). Investigation of normal nodes. *J. Marine Res. 16,* 109–144.

Richtmyer, R. D. & Morton, K. W. 1967. *Difference method for initial value problem.* New York: Interscience Publication, pp. 405.

de Rivas, E. V. 1972. On the use of nonuniform grids in finite difference equations. *J. Comput. Phys. 10,* 202–210.

Roll, H. V. 1965. *Physics of the marine atmosphere.* New York: Academic Press, pp. 152–160.

Schloemer, R. W. 1954. *Analysis and synthesis of hurricane wind pattern over Lake Okeechobee, Florida.* Hydrometeorological Rept. No. 31, U.S. Weather Bureau, 49 pp.

Suginohara, N. 1973. Response of a two-layer ocean to typhoon passage in the western boundary region. *J. Oceanog. Soc. Japan 29,* 236–250.

ЧИСЛЕННОЕ ИЗУЧЕНИЕ РЕАКЦИИ БАРОТРОПНОГО ОКЕАНА НА ДВИЖУЩИЙСЯ ТАЙФУН

Численно изучается реакция баротропного океана на движущийся тайфун для прямоугольного океана постоянной глубины с шельфовыми зонами по бокам. Определяются крупномасштабные характеристики изменений уровня океана и циркуляции, хотя модель описывает и мезомасштабные явления, подобные шельфовым волнам. В открытом океане изменения уровня океана обусловлены, главным образом, низким давлением, в то же время напряжение ветра приводит к интенсивным течениям. Возмущение над открытым океаном сопровождается вынужденными волнами и оставляет после себя геострофически сбалансированное течение. Когда возмущение находится далеко от берега, прибрежная область испытывает только слабые инерционно-гравитационные колебания. Внезапное изменение уровня океана и возрастание скорости имеют место, когда возмущение проходит шельфовую зону. По мере того, как возмущение удаляется в открытое море, вынужденные волны становятся свободными шельфовыми волнами, которые распространяются вдоль берега по часовой стрелке. Результаты вычислений сравниваются с данными наблюдений об изменениях уровня океана вдоль берега и изменениях температуры в океане после прохождения возмущения.